

# Acetone Oxidation Using Ozone on Manganese Oxide Catalysts

Yan Xi, Corey Reed, Yong-Kul Lee, and S. Ted Oyama\*

Environmental Catalysis and Nanomaterials Laboratory, Department of Chemical Engineering,  
Virginia Tech, Blacksburg, Virginia 24061

Received: June 2, 2005; In Final Form: July 14, 2005

Supported manganese oxide catalysts were prepared by the impregnation of alumina foam blocks washcoated with alumina and silica. The manganese content based on the weight of the washcoats was 10 wt % calculated as  $\text{MnO}_2$ . Fourier transform profiles of the Mn K-edge EXAFS spectra for these samples gave three distinctive peaks at 0.15, 0.25, and 0.32 nm and were close to the profiles of  $\text{Mn}_3\text{O}_4$  and  $\beta\text{-MnO}_2$ . The number of surface active sites was determined through oxygen chemisorption measurements at a reduction temperature ( $T_{\text{red}} = 443 \text{ K}$ ) obtained from temperature-programmed reduction (TPR) experiments. Acetone catalytic oxidation was studied from room temperature to 573 K, and was found to be highly accelerated by the use of ozone on both catalysts with substantial reductions in the reaction temperature. The only carbon-containing product detected was  $\text{CO}_2$ . The alumina-supported catalyst was found to be more active than the silica-supported catalyst in acetone and ozone conversion, with higher turnover frequencies (TOFs) for both reactions. The pressure drop through the foam was low and increased little ( $0.003 \text{ kPa}/10\,000 \text{ h}^{-1}$ ) with space velocity. In situ steady-state Raman spectroscopy measurements during the acetone catalytic oxidation reaction showed the presence of an adsorbed acetone species with a C–H bond at  $2930 \text{ cm}^{-1}$  and a peroxide species derived from ozone with an O–O bond at  $890 \text{ cm}^{-1}$ .

## Introduction

Catalytic oxidation is a promising method to control the emission of volatile organic compounds (VOCs), a class of airborne pollutants with harmful effects on human health and the environment. The U.S. Environmental Protection Agency defines VOCs as compounds of carbon that have high photochemical activity while excluding pure carbon, carbonate carbon, solid carbide compounds in which the carbon is bonded to a metal, CO, and  $\text{CO}_2$ .<sup>1</sup> The use of ozone as an alternative oxidant for the catalytic oxidation of VOCs<sup>2–5</sup> and gaseous reduced sulfur compounds<sup>6</sup> has been reported in the literature. Ozone is an allotropic form of oxygen with strong oxidizing power exceeded only by fluorine, the perxenite ion, atomic oxygen, OH radicals, and a few other such species.<sup>7</sup>

The use of ozone to reduce the conversion temperature for VOCs is important in air pollution control because it obviates the need for heating and then cooling large volumes of air. Naydenov et al.<sup>8</sup> studied the kinetics of complete oxidation of benzene over  $\text{MnO}_2$  using ozone. They found that the decomposition of ozone and the oxidation of benzene occurred in the same range (283–353 K) while the oxidation of benzene with oxygen took place at higher temperatures ( $>433 \text{ K}$ ). They also found that the apparent activation energy for ozone decomposition (32 kJ/mol) was similar to that of benzene oxidation using ozone (30 kJ/mol), and was lower than that of benzene oxidation using oxygen (88 kJ/mol). Oyama et al.<sup>9</sup> compared the catalytic oxidation of ethanol over supported molybdenum and manganese oxide catalysts and found similar trends. For a 10 wt %  $\text{MnO}_2/\text{Al}_2\text{O}_3$  catalyst the activation energy with ozone (3.7 kJ/mol) was lower than that with oxygen (89 kJ/mol) and occurred at lower temperatures ( $<400 \text{ K}$ ). For a 9 wt %  $\text{MoO}_3/\text{SiO}_2$  catalyst the activation energy for the reaction with ozone (10

kJ/mol) was similarly lower than that with oxygen (92 kJ/mol) and also occurred at low temperatures ( $<523 \text{ K}$ ). A significant difference was that the  $\text{MnO}_2$  produced mainly carbon dioxide while the  $\text{MoO}_3$  formed mostly acetaldehyde. Thus, the nature of the catalyst played a significant role in the reaction pathway. In another study Ragaini et al.<sup>5</sup> investigated the oxidation of VOCs with and without ozone over a barium-promoted copper-chromite catalyst. They reported that styrene was more easily destroyed with ozone and that the conversion of styrene to a desired concentration (50 ppm) required a lower temperature ( $<388 \text{ K}$ ) with ozone than with oxygen ( $>523 \text{ K}$ ). Hutchings et al.<sup>10</sup> found that ozone was more active than oxygen for methane oxidation over an alumina-supported magnesium oxide catalyst.

Both supported noble metals (Pd and Pt) and transition metal oxides (Mn, Cr, Fe) have been reported as catalysts in the catalytic elimination of VOCs.<sup>3,11</sup> The catalysts employed in this study were manganese oxide supported on silica and alumina washcoats deposited on aluminum oxide foam substrates to provide good mixing and low-pressure drop.<sup>12</sup> Manganese oxide was chosen as the catalyst because it is a well-known complete oxidation catalyst for VOCs<sup>13</sup> and is also an active catalyst for ozone decomposition.<sup>12</sup> Kim et al.<sup>14</sup> found that Mn oxide had higher activity than Cu, Mo, Fe, V, Co, Ni, and Zn oxides supported on  $\gamma\text{-Al}_2\text{O}_3$  for the total oxidation of toluene. Mn oxide was also reported to have a higher ozone decomposition rate than Co, Ni, Cr, Ag, Cu, Ce, Fe, V, and Mo oxides,<sup>12</sup> and detailed studies of the mechanism of decomposition on Mn oxide have been carried out.<sup>15,16</sup>

The VOC used in this study was acetone, which is a common solvent used in many industrial processes such as surface coating, painting, and extraction. Similar to other VOCs, acetone is harmful to human health. Acetone has been studied in the literature as an example of a VOC containing a carbonyl

\* To whom correspondence should be addressed. E-mail: oyama@vt.edu.

**TABLE 1: Sample Weight Summary for Each Step in the Foam Catalyst Preparation**

catalyst samples	wt of blank foam, g	wt of washcoated sample, g	wt of washcoat, g	wt of final sample, g	wt of MnO <sub>x</sub> , g	wt % of MnO <sub>x</sub> (washcoat)
10 wt % MnO <sub>x</sub> /SiO <sub>2</sub>	20.123	21.975	1.852	22.190	0.215	10.4
10 wt % MnO <sub>x</sub> /Al <sub>2</sub> O <sub>3</sub>	23.308	23.308	4.294	23.820	0.512	10.7
Si coated foam	19.083	20.628	1.545			
Al coated foam	19.968	22.167	2.199			

group.<sup>3,5,17,18</sup> Baldi et al.<sup>19</sup> found that the conversion of acetone with excess oxygen over Mn<sub>3</sub>O<sub>4</sub> started at near 473 K, with acetaldehyde being the main product, together with minor amounts of acetic acid. The conversion increased to high values in the temperature range of 510–563 K where the only carbon-containing product was CO<sub>2</sub>. Parida and Samal<sup>18</sup> used manganese nodules collected from the Indian Ocean in the combustion with oxygen of VOCs, including acetone, and found that complete oxidation of acetone was achieved at a temperature less than 573 K. Ragaini et al.<sup>5</sup> reported that the oxidation temperature of acetone on barium-promoted copper-chromite catalyst decreased by 10% when ozone was used in the reaction instead of oxygen.

In this work the catalytic active phase was placed on alumina foam substrates. These are monolithic materials with a three-dimensional, interconnected macropore structure possessing low densities and novel physical, mechanical, and thermal properties that offer potential application as catalyst supports.<sup>20–23</sup> Dhandapani et al.<sup>12</sup> compared the pressure drop in pellets, monoliths, and foams with the same geometric surface area of 620 cm<sup>2</sup> and found that the monolith and foam had a similar low gas resistance compared to the pellets. The catalytic performance of the straight pore monolith and the foam were the same, suggesting that the foam could be employed instead of the commonly used monolith. Patcas<sup>24</sup> studied the methanol-to-olefins conversion over zeolite-coated ceramic foams and found that the use of the foams as carriers allowed variation of the catalyst bulk thickness with almost no influence on the hydrodynamics, and at the same time provided high turbulence and radial mixing.

This work compares the activities of silica- and alumina-supported manganese oxide catalysts deposited on foam substrates for the oxidation of acetone. The use of ozone resulted in a significant reduction in the reaction temperature and increase in reaction rate.

## Experimental Section

**Catalyst Preparation.** The substrate material for the catalyst was a monolithic aluminum oxide foam (Amporex, Fiber-Ceramics, Inc., Cincinnati, OH) cut into a cylindrical shape of 3.5 cm diameter and 1.3 cm height and approximately 20 g in weight. The original pore density of the foam was a nominal 30 pores per inch (ppi). The catalysts (10 wt % MnO<sub>x</sub>/SiO<sub>2</sub> and 10 wt % MnO<sub>x</sub>/Al<sub>2</sub>O<sub>3</sub>) were prepared by a multiple impregnation method. The foam substrates were first washcoated with SiO<sub>2</sub> (Cabot, Cabosil LM130, 134 m<sup>2</sup> g<sup>-1</sup>) and Al<sub>2</sub>O<sub>3</sub> (Degussa Aluminumoxid C, 96 m<sup>2</sup> g<sup>-1</sup>) powders using a slurry of 18.0 g of silica in 150 mL of water and a slurry of 15.3 g of alumina in 100 mL of water. The foams were placed in the slurry solutions for approximately 30 s, removed, and shaken to remove as much residual liquid as possible, and were then dried at 393 K for 6 h and calcined at 773 K for 8 h in an oven provided with good air circulation. Three or more coating/heating cycles were used to get the washcoated sample. The amount of washcoat was obtained from the gain in weight of the original foam by application of the washcoat, and typically

was about 2.0–4.0 g (1–2%) for alumina and 1.5–2.0 g (0.7–1%) for silica. Finally the coated foams were impregnated with an aqueous solution of the precursor manganese(II) acetate tetrahydrate (Aldrich, 99.99%). The samples were dipped into the solution quickly, and then shaken to remove the excess solution, dried at 393 K for 6 h, and calcined at 773 K for 8 h. The impregnation solution was not completely utilized, but using a 2-fold excess of the manganese precursor (5.1 and 2.5 g of manganese acetate respectively for alumina and silica in 200 cm<sup>3</sup> of water) gave approximately 10 wt % of MnO<sub>2</sub> based on the weight of the two washcoats. Typical weights of the original foams, washcoats, and the final loadings based on the washcoats are presented in Table 1.

Another 10 wt % manganese oxide on silica catalyst was prepared for the Raman spectroscopy experiments by the incipient wetness impregnation method using an aqueous solution of manganese acetate (Aldrich, 99.99%) added dropwise to a previously calcined (773 K for 6 h) support, SiO<sub>2</sub> (Cabot, Cabosil EH-5, 320 m<sup>2</sup>/g). After impregnation, the sample was dried at 393 K for 6 h and then was calcined at 773 K for 6 h at a heating rate of 0.83 K/s (5 K/min). This sample was denoted 10 wt % MnO<sub>x</sub>/SiO<sub>2</sub>-H to indicate that it was prepared on a higher surface area silica, and to distinguish it from the sample obtained on the foam substrate.

**Characterization.** The foam samples were crushed and ground to fine powders for BET, temperature-programmed reduction (TPR), and oxygen chemisorption measurements. For other analyses, the washcoat containing the supported manganese oxide was knocked off the foam structure and ground into fine powders.

X-ray diffraction (XRD) patterns were obtained with an ASC-0007 model diffractometer using Cu Kα radiation generated at 45 kV and 40 mA. The measurements were obtained at a 2θ angle range of 10° to 90° using a scanning rate of 0.03 deg/s (2 deg/min).

Extended X-ray absorption fine structure (EXAFS) spectroscopy measurements were carried out in transmission mode at the X18B beam line of the NSLS (National Synchrotron Light Source) with a 2.5 GeV ring energy and 300–400 mA ring current. The beam line used a Si (111) crystal monochromator and gave an energy resolution of 2 eV. WinXas 2.3 software was used to analyze the EXAFS results. Samples (0.5 g) were pretreated in a 20% oxygen/helium mixture at 723 K for 3 h and then transferred into cells with Kapton windows without exposure to the atmosphere.

Temperature-programmed reduction (TPR) and oxygen chemisorption measurements were carried out in a standard flow system equipped with a computer interfaced mass spectrometer (Dycor/Ametek Model MA 100). The samples (0.2 g) were pretreated at 773 K for 2 h in 54 μmol/s (80 cm<sup>3</sup>/min) of oxygen (Air Products, >99.6%) flow to remove excess moisture and carbon impurities. Then the samples were reduced in 68 μmol/s (100 cm<sup>3</sup>/min) of hydrogen (Air Products, >99.6%) flow from room temperature to 1073 K at a rate of 0.03 K/s (2 K/min). The mass spectrometer signal of H<sub>2</sub>O<sup>+</sup> (*m/e* 18) was monitored during the reduction process to determine the reduction tem-

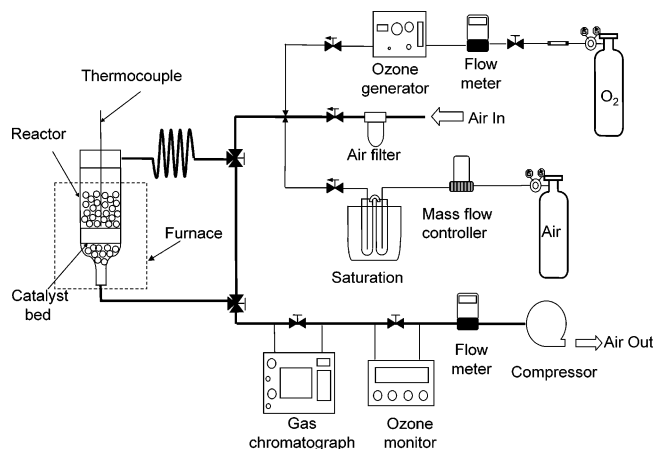


**Figure 1.** Schematic of the acetone oxidation reaction system.

perature ( $T_{\text{red}}$ ), which was taken to be the temperature right before the onset of bulk reduction. Experimentally, this was the point at which the signal increased dramatically in the TPR trace. Oxygen chemisorption was performed at this reduction temperature.

Irreversible oxygen chemisorption was measured by a pulse technique following pretreatment of the catalyst at 773 K for 2 h in  $54 \mu\text{mol/s}$  ( $80 \text{ cm}^3/\text{min}$ ) of oxygen (Air Products, >99.6%) and reduction in  $68 \mu\text{mol/s}$  ( $100 \text{ cm}^3/\text{min}$ ) of hydrogen (Air Products, >99.6%) at  $T_{\text{red}}$  for 2 h. After reduction the flow was switched to  $68 \mu\text{mol/s}$  ( $100 \text{ cm}^3/\text{min}$ ) of helium (Air Products, >99.6%) at the same temperature and pulses ( $19.56 \mu\text{mol}$ ) of oxygen were injected into the reactor while monitoring the intensity of the  $\text{O}_2^+$  signal. Dispersion was calculated based on the amount of atomic oxygen uptake and the total amount of manganese loaded on the sample.

Brunauer–Emmett–Teller (BET) surface area measurements were carried out in an automatic volumetric adsorption apparatus (Micromeritics, ASAP 2010) using 0.2 g samples loaded into a quartz reactor and degassed at 423 K in a vacuum prior to measurement. A five-point  $\text{N}_2$  (Air Products, >99.6%) analysis method was used to determine the surface area of each sample.

**Reactivity Measurements.** The acetone oxidation reaction was carried out in a flow reactor system (Figure 1) using a 3.5 cm i.d. tubular fixed-bed quartz reactor at atmospheric pressure. The cylindrical foam catalysts (7.314 g of 10 wt %  $\text{MnO}_x/\text{SiO}_2$  and 6.738 g of 10 wt %  $\text{MnO}_x/\text{Al}_2\text{O}_3$ ) were wedged into the middle of the tube with quartz tape to prevent gas bypass. The volumes below and above the catalysts were packed with glass spheres to minimize the residence time of the gas in the empty reactor space and to achieve efficient preheating of the reactants. The pressure drop across the sample was measured with a digital pressure gauge (Mensor, DPG II, Model 15000) with switchable inlets before and after the reactor. The main flow stream was air purified by passage through a Balston filter (Whatman Inc., Model 912) and drawn through the system by a compressor (Shizoki, Japan, Model WME-RS) located at the exit of the system. The total flow rate was controlled by a variable autotransformer (Staco Energy Products Co., Dayton, OH, Type 3PN1010) connected to the compressor, and was measured by a flow meter (Top Trak, Series 820). Ozone was produced by passing oxygen (Air products, >99.6%) through a corona discharge in a high voltage ozone generator (OREC, V5-0) and was introduced in an independent line. The ozone concentration was monitored via an ozone monitor (In USA, Model H1) with a UV lamp detector. Acetone was introduced through another independent line using a two-stage bubbler placed inside an ice

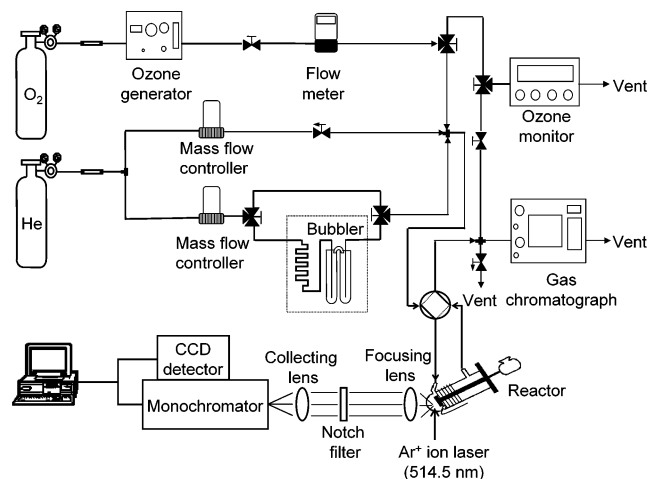


**Figure 2.** Schematic of the in situ laser Raman spectroscopy system.

bath with a temperature of 273 K. The overall acetone concentration was set by regulating the air (Air Products, >99.6%) flow through the bubbler with a mass flow controller. The acetone vapor pressure (9.25 kPa) was calculated from Antoine's equation (see Appendix).

A gas chromatograph (GC) (HP 5890A) equipped with a flame ionization detector with a Chrom W-AW 80/100 column (Alltech, 6 ft  $\times$  1/8 in.  $\times$  0.085 in. SS) and a thermal conductivity detector with a Haysep A 80/100 packed column (Alltech, 36 ft  $\times$  1/8 in.  $\times$  0.085 in. at steel) was used to measure the concentration of the acetone, CO, and  $\text{CO}_2$ . The GC was capable of detecting other organic compounds such as acetic acid, acetaldehyde, methanol, methane, ethane, ethylene, and acetylene. Importantly, in the catalytic testing, points were taken at increasing and decreasing temperatures to establish catalyst stability. Measurements were taken after 0.5 h, which was sufficient to obtain steady-state conditions. The conditions for the reactivity measurements are summarized in Table 2.

**Raman Spectroscopic Measurements.** The in situ laser Raman spectroscopy experiments were performed on the powder 10 wt %  $\text{MnO}_x/\text{SiO}_2$ -H catalyst to monitor the adsorbed intermediates resulting from the reaction between acetone and ozone. The schematic is shown in Figure 2. The spectroscopic part of the system was made up of an argon ion laser (514.5 nm, Spex Lexcel 95) as a light source, a holographic notch filter (Kaiser, Super Notch Plus) to reduce Rayleigh scattering, a single stage monochromator (Spex, 500 M) for the energy dispersion of the light, and a CCD detector (Spex, Spectrum One) for spectral acquisition. The detector slit width was set at  $100 \mu\text{m}$  giving a resolution of  $6 \text{ cm}^{-1}$ . The laser was operated at around 160 mW giving a power at the sample of 140 mW.

The powder catalyst sample was pressed into a thin wafer of 0.1 cm thickness and 1.5 cm diameter and was held in place by a stainless steel cap at the end of a ceramic rod. The rod was rotated at 1800 rpm to prevent thermal degradation of the sample by the laser and was enclosed by a synthetic quartz (Suprasil) cell provided with heating tape and inlet and outlet ports, so as to serve as an in situ reactor. The catalyst temperature was measured by a thermocouple that was placed in a well 3 mm from the sample. Laser light was focused onto the sample, and the scattered radiation was collected by a lens, filtered, and sent on to the monochromator. The reactor part of the system was attached to the Raman spectrometer and was similar to the one used in the foam testing system. It included a gas delivery system equipped with a two-stage bubbler for the vaporization of liquid acetone, a high voltage ozone generator (OREC, V5-



TABLE 2: Summary of Reaction Conditions for Different Experiments.

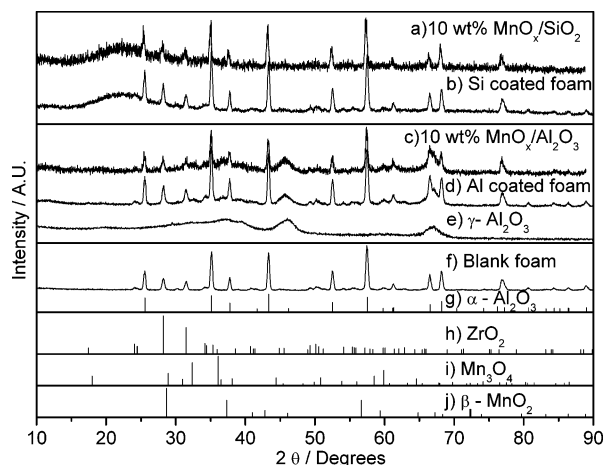
experiment	catalyst	reaction concn	reaction conditions			note
			$F_{\text{tot}}$ , L/min	SV/h <sup>-1</sup>	T/K	
acetone oxidation with O <sub>2</sub>	blank foam	[acet] = 0.1 mol % (1 000 ppm)	3.1	15 000	RT–573	Figure 6
	10 wt % MnO <sub>x</sub> /SiO <sub>2</sub>					
	10 wt % MnO <sub>x</sub> /Al <sub>2</sub> O <sub>3</sub>					
acetone oxidation with O <sub>3</sub>	blank foam	[acet] = 0.1 mol % (1 000 ppm)	3.1	15 000	RT–573	Figure 6
	10 wt % MnO <sub>x</sub> /SiO <sub>2</sub>					Figure 7
	10 wt % MnO <sub>x</sub> /Al <sub>2</sub> O <sub>3</sub>					Figure 8
O <sub>3</sub> decomposition	blank foam	[O <sub>3</sub> ] = 0–0.8 mol % (8 000 ppm)	3.1	15 000	RT–573	Figure 7
	10 wt % MnO <sub>x</sub> /SiO <sub>2</sub>					
	10 wt % MnO <sub>x</sub> /Al <sub>2</sub> O <sub>3</sub>					
pressure drop over foam catalyst	blank foam	[acet] = 0.1 mol % (1 000 ppm)	2.1–6.3	10 000–30 000	325	Figure 9
	10 wt % MnO <sub>x</sub> /SiO <sub>2</sub>					
	10 wt % MnO <sub>x</sub> /Al <sub>2</sub> O <sub>3</sub>					
Raman spectroscopy	10 wt % MnO <sub>x</sub> /SiO <sub>2</sub> -H	[acet] = 0.2 mol % (2 000 ppm) [O <sub>3</sub> ] = 1.0 mol % (10 000 ppm)	0.5	170 000	303–373	Figure 10
						Figure 11
						Figure 12

0), an ozone monitor (In USA, Model H1), and a gas chromatograph (GC) (SRI, Model 8610C).

The sample was pretreated at 723 K for 2 h in an oxygen and helium stream to remove excess moisture and other impurities from the sample. The conditions of measurement are summarized in Table 2.

## Results

**Catalysts Characterization Results.** Figure 3 shows the X-ray diffraction results for the catalyst samples, the foam substrates with the two different washcoats, the blank foam, and the  $\gamma$ -Al<sub>2</sub>O<sub>3</sub>. The references  $\alpha$ -Al<sub>2</sub>O<sub>3</sub> (PDF 10-173), ZrO<sub>2</sub> (PDF 24-1165), Mn<sub>3</sub>O<sub>4</sub> (PDF 800382), and  $\beta$ -MnO<sub>2</sub> (PDF 24-0735) are also presented. For both the silica-supported catalyst and the silica washcoated foam there is one broad peak located at around 23° due to amorphous silica. For the alumina-supported catalyst and the alumina washcoated foam there are three broad features at around 36°, 46°, and 66° corresponding to  $\gamma$ -Al<sub>2</sub>O<sub>3</sub>. For the foam structure, most of the peaks are attributed to  $\alpha$ -Al<sub>2</sub>O<sub>3</sub>, but the other features located at 28°, 32°, 49°, and 52° are due to an additional component, ZrO<sub>2</sub>, which is contained inside the foam. The catalyst samples do not show any peaks due to manganese oxides indicating that the supported phase is well dispersed.



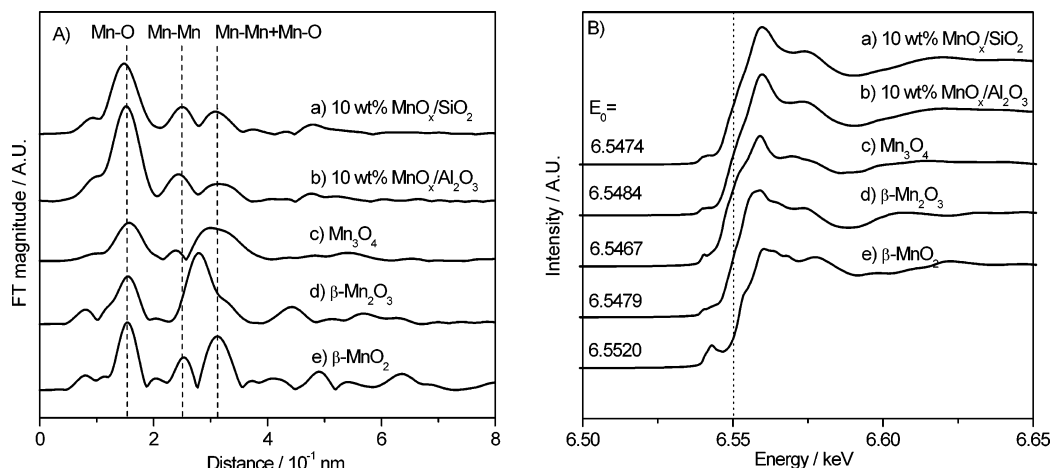
**Figure 3.** XRD results: (a) 10 wt % MnO<sub>x</sub>/SiO<sub>2</sub>, (b) Si coated foam, (c) 10 wt % MnO<sub>x</sub>/Al<sub>2</sub>O<sub>3</sub>, (d) Al coated foam, (e)  $\gamma$ -Al<sub>2</sub>O<sub>3</sub>, (f) blank foam, (g)  $\alpha$ -Al<sub>2</sub>O<sub>3</sub> (PDF 10-173), (h) ZrO<sub>2</sub> (PDF 24-1165), (i) Mn<sub>3</sub>O<sub>4</sub> (PDF 800382), and (j)  $\beta$ -MnO<sub>2</sub> (PDF 24-0735).

Figure 4a shows the Fourier transforms of the Mn K-edge EXAFS spectra for the two catalysts and three references: (a) 10 wt % MnO<sub>x</sub>/SiO<sub>2</sub>, (b) 10 wt % MnO<sub>x</sub>/Al<sub>2</sub>O<sub>3</sub>, (c) Mn<sub>3</sub>O<sub>4</sub>, (d)  $\beta$ -Mn<sub>2</sub>O<sub>3</sub>, and (e)  $\beta$ -MnO<sub>2</sub>. The transforms for all the samples have a broad peak at around 0.15 nm corresponding to a Mn–O bond. The transforms of the catalysts,  $\beta$ -MnO<sub>2</sub>, and Mn<sub>3</sub>O<sub>4</sub> also have a peak at around 0.25 nm corresponding to a Mn–Mn distance and a broad peak at around 0.32 nm due to contributions from Mn–O and Mn–Mn bonds. The profile of  $\beta$ -Mn<sub>2</sub>O<sub>3</sub> shows a second peak at around 0.28 nm due to contributions from Mn–O and Mn–Mn bonds. Figure 4b shows the corresponding Mn K-edge XANES spectra for the two catalysts and three references. The absorption edge energy ( $E_0$ ) values for those samples are also displayed in this figure. The  $E_0$  for the 10 wt % MnO<sub>x</sub>/SiO<sub>2</sub> (6.5474 keV) is close to that of the Mn<sub>3</sub>O<sub>4</sub> (6.5467 keV), and the  $E_0$  for the 10 wt % MnO<sub>x</sub>/Al<sub>2</sub>O<sub>3</sub> (6.5484 keV) is close to that of the  $\beta$ -Mn<sub>2</sub>O<sub>3</sub> (6.5479 keV).

Figure 5 shows the H<sub>2</sub>O<sup>+</sup> ( $m/e$  18) TPR traces for the 10 wt % MnO<sub>x</sub>/SiO<sub>2</sub> and the 10 wt % MnO<sub>x</sub>/Al<sub>2</sub>O<sub>3</sub> foam catalysts. For both samples the traces show an initial reduction peak of manganese oxide at around 493 K and a second reduction peak at around 571 K. They also both have the same onset reduction temperature ( $T_{\text{red}} = 443$  K). For the Al<sub>2</sub>O<sub>3</sub>-supported sample, there is a small feature at low temperature (<373 K), which may be due to adsorbed water. Oxygen uptake and dispersion values for the two catalysts (10 wt % MnO<sub>x</sub>/SiO<sub>2</sub> and 10 wt % MnO<sub>x</sub>/Al<sub>2</sub>O<sub>3</sub>) along with the corresponding surface area results based on the overall sample weight and the weight of the washcoat are summarized in Table 3. The surface areas of the washcoated foams and a blank foam are also reported.

**Reactivity Results.** Three series of experiments were performed on the 10 wt % MnO<sub>x</sub>/SiO<sub>2</sub> catalyst, 10 wt % MnO<sub>x</sub>/Al<sub>2</sub>O<sub>3</sub> catalyst, and the blank alumina foam: (a) acetone oxidation using an ozone/oxygen mixture, (b) acetone oxidation using oxygen alone, and (c) ozone decomposition.

A summary of conditions is given in Table 2. The total flow rate was kept at 3.1 L/min (space velocity = 15 000 h<sup>-1</sup>) except in experiments where the space velocity was varied. The acetone oxidation studies were carried out with a fixed acetone concentration of 0.10 mol % (1 000 ppm) and varying ozone concentrations of 0–0.80 mol % (0–8 000 ppm) corresponding to ozone/acetone molar ratios ( $R$ ) ranging from 0 to 8. The ozone decomposition studies used an ozone concentration of 0.50 mol



**Figure 4.** (a) Fourier transforms of the Mn K-edge EXAFS spectra and (b) corresponding Mn K-edge XANES spectra: (a) 10 wt %  $\text{MnO}_x/\text{SiO}_2$ , (b) 10 wt %  $\text{MnO}_x/\text{Al}_2\text{O}_3$ , (c)  $\text{Mn}_3\text{O}_4$ , (d)  $\beta\text{-Mn}_2\text{O}_3$ , and (e)  $\beta\text{-MnO}_2$ .

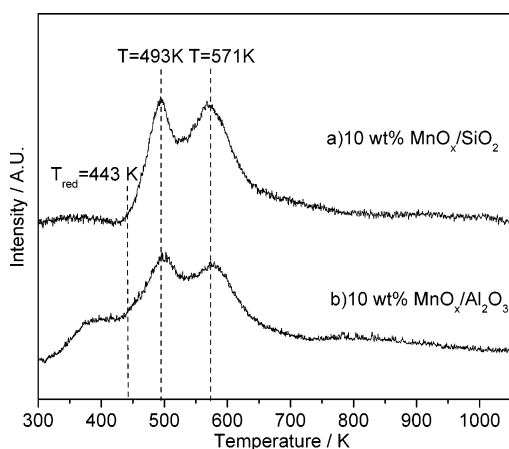


**Figure 5.** TPR traces ( $m/e$  18) for (a) of 10 wt %  $\text{MnO}_x/\text{SiO}_2$  and (b) 10 wt %  $\text{MnO}_x/\text{Al}_2\text{O}_3$ .

% (5 000 ppm). Catalyst activity was studied as a function of temperature ranging from room temperature to 573 K. The ozone concentration for the reactions presented in Figures 6 and 7 was 5 000 ppm corresponding to an ozone/acetone molar ratio of 5. In the oxidation reactions  $\text{CO}_2$  was the only carbon-containing product observed. The turnover frequencies (TOFs) were calculated for both acetone and ozone conversion with use of the oxygen uptake values from the oxygen chemisorption experiments and the conversion values.

The effect of temperature on acetone conversion and TOFs are presented in Figure 6. Blank acetone oxidation reactions were carried out over the alumina foam with and without ozone. With just air the acetone conversion was less than 10% even above 550 K (Figure 6a). With ozone present acetone reacted on the alumina foam at temperatures higher than 450 K but at much lower conversion than on the  $\text{MnO}_x$  catalysts. The conversion of acetone for the reaction with air over the 10 wt %  $\text{MnO}_x/\text{Al}_2\text{O}_3$  and 10 wt %  $\text{MnO}_x/\text{SiO}_2$  catalysts (Figure 6a) occurred at temperatures higher than 450 K over both catalysts.

The conversion of acetone for the reaction with ozone over the 10 wt %  $\text{MnO}_x/\text{Al}_2\text{O}_3$  and 10 wt %  $\text{MnO}_x/\text{SiO}_2$  catalysts (Figure 6a) occurred already at room temperature. Figure 6b shows the corresponding TOFs for acetone over the two catalysts.

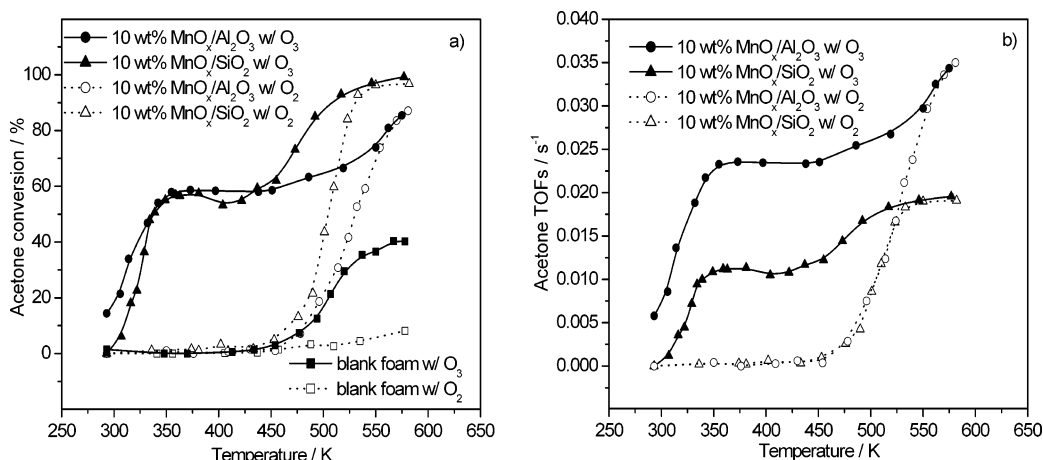
The effect of temperature on ozone decomposition conversion and TOFs are shown in Figure 7. Again, blank reactions of ozone decomposition over the alumina foam with and without acetone were performed and the results are shown in Figure 7a. On the foam substrate ozone decomposed at temperatures higher than 350 K without acetone and at temperatures higher than 450 K with acetone. Ozone conversions over the 10 wt %  $\text{MnO}_x/\text{Al}_2\text{O}_3$  and 10 wt %  $\text{MnO}_x/\text{SiO}_2$  catalysts with and without acetone (Figure 7a) show that ozone starts to decompose from room temperature and is totally decomposed at temperatures higher than 350 K for the 10 wt %  $\text{MnO}_x/\text{SiO}_2$  catalyst and higher than 400 K for the 10 wt %  $\text{MnO}_x/\text{Al}_2\text{O}_3$  catalyst. The corresponding TOFs of ozone decomposition over the two catalysts are presented in Figure 7b. For the alumina-supported sample the rate of the ozone reaction is higher in the presence of ozone, which as will be discussed indicates that the reacting acetone captures surface oxygen species derived from ozone.

Figure 8 shows the effects of ozone concentration on acetone conversion on the (a) 10 wt %  $\text{MnO}_x/\text{SiO}_2$  and (b) 10 wt %  $\text{MnO}_x/\text{Al}_2\text{O}_3$  catalysts. In these reactions the ozone/acetone molar ratio ( $R$ ) was varied and ranged from 0 to 8, and the conversion of acetone increased with increasing ozone concentration. An acetone conversion around 70% was obtained by using an  $R$  of 8 at 350 K on both catalysts.

The effect of space velocity on acetone and ozone conversion as well as pressure drop was also tested over the silica-supported catalyst. In these reactions, the acetone concentration was again 1 000 ppm, the ozone concentration was 5 000 ppm, and the reaction temperature was 325 K. The space velocity varied from 10 000 to 30 000  $\text{h}^{-1}$  corresponding to total flow rates ranging from 2.1 to 6.3 L/min. Figure 9a shows the effect of space

**TABLE 3: Surface Area, Oxygen Chemisorption, and Dispersion Values.**

catalyst	$T_{\text{red}}$ , K	S.A., $\text{m}^2$ (g sample) $^{-1}$	S.A., $\text{m}^2$ (g washcoat) $^{-1}$	$\text{O}_2$ uptake, $\mu\text{mol (g sample)}^{-1}$	$\text{O}_2$ uptake, $\mu\text{mol (g washcoat)}^{-1}$	dispersion, %
10 wt % $\text{MnO}_x/\text{SiO}_2$	443	21	250	7.3	87	7.2
10 wt % $\text{MnO}_x/\text{Al}_2\text{O}_3$	443	23	130	3.9	22	6.3
10 wt % $\text{MnO}_x/\text{SiO}_2\text{-H}$		320		49		8.4
Al coated foam		39	390			
Si coated foam		61	810			
foam		5.0				



**Figure 6.** (a) Acetone conversion versus temperature and (b) TOF versus temperature for the 10 wt % MnO<sub>x</sub>/SiO<sub>2</sub>, 10 wt % MnO<sub>x</sub>/Al<sub>2</sub>O<sub>3</sub> catalysts and blank foam in the presence and absence of ozone: (□) blank foam without ozone; (■) blank foam with ozone; (Δ) 10 wt % MnO<sub>x</sub>/SiO<sub>2</sub> without ozone; (○) 10 wt % MnO<sub>x</sub>/Al<sub>2</sub>O<sub>3</sub> without ozone; (▲) 10 wt % MnO<sub>x</sub>/SiO<sub>2</sub> with ozone; (●) 10 wt % MnO<sub>x</sub>/Al<sub>2</sub>O<sub>3</sub> with ozone.  $F_{\text{tot}} = 3.1$  L/min, space velocity = 15 000 h<sup>-1</sup>, acetone concentration = 1 000 ppm, ozone concentration = 5 000 ppm.

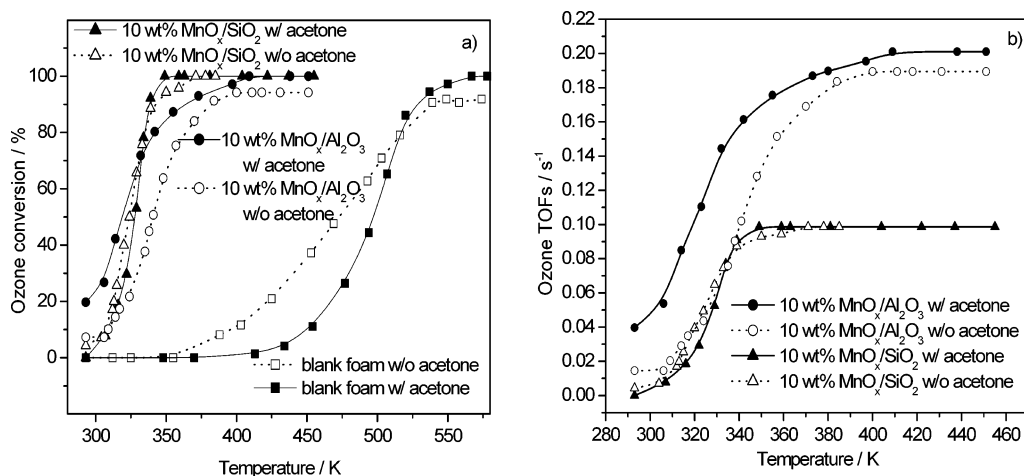


**Figure 7.** (a) Ozone conversion versus temperature and (b) TOF versus temperature for the 10 wt % MnO<sub>x</sub>/SiO<sub>2</sub>, 10 wt % MnO<sub>x</sub>/Al<sub>2</sub>O<sub>3</sub> catalysts and blank foam in the presence and absence of acetone: (■) blank foam with acetone; (□) blank foam without acetone; (○) 10 wt % MnO<sub>x</sub>/Al<sub>2</sub>O<sub>3</sub> without acetone; (●) 10 wt % MnO<sub>x</sub>/Al<sub>2</sub>O<sub>3</sub> with acetone; (Δ) 10 wt % MnO<sub>x</sub>/SiO<sub>2</sub> without acetone; (▲) 10 wt % MnO<sub>x</sub>/SiO<sub>2</sub> with acetone.  $F_{\text{tot}} = 3.1$  L/min, space velocity = 15 000 h<sup>-1</sup>, acetone concentration = 1 000 ppm, ozone concentration = 5 000 ppm.

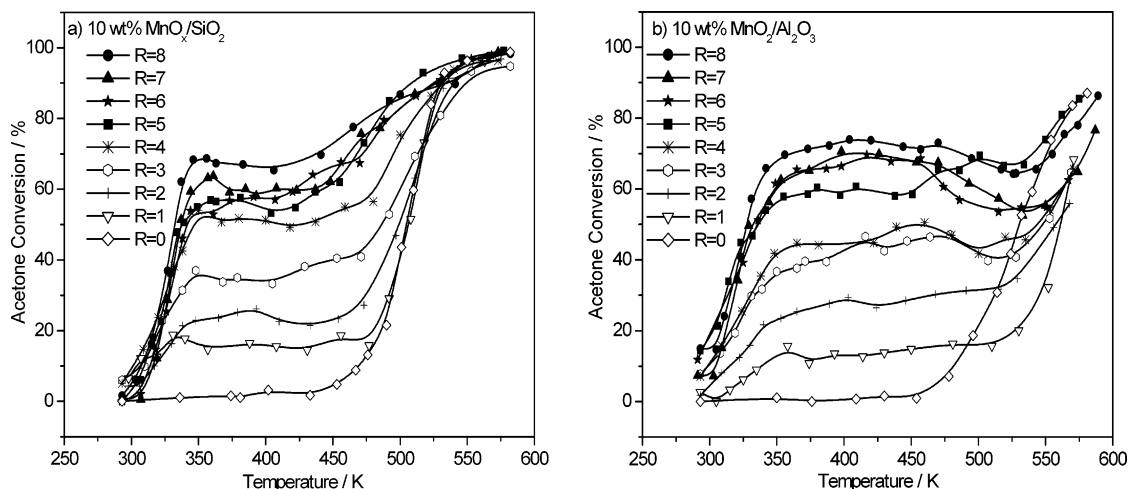


**Figure 8.** Acetone conversion versus temperature for 10 wt % MnO<sub>x</sub>/SiO<sub>2</sub> and 10 wt % MnO<sub>x</sub>/Al<sub>2</sub>O<sub>3</sub> catalysts with various ozone concentrations: (a) 10 wt % MnO<sub>x</sub>/SiO<sub>2</sub> and (b) 10 wt % MnO<sub>x</sub>/Al<sub>2</sub>O<sub>3</sub>.  $R$  is the ozone/acetone molar ratio.  $F_{\text{tot}} = 3.1$  L/min, space velocity = 15 000 h<sup>-1</sup>, acetone concentration = 1 000 ppm, ozone concentration = 1 000–8 000 ppm.

velocity on the acetone reaction with ozone over the silica-supported catalyst, and Figure 9b shows the effect of space velocity on pressure drop. The conversion of acetone and ozone increased with decreasing space velocity, and the pressure drop

increased with increasing space velocity. Figure 9b also displays the theoretical results calculated from the Ergun equation for ceramic foams.<sup>25</sup> Details of the calculations are presented in the Appendix.

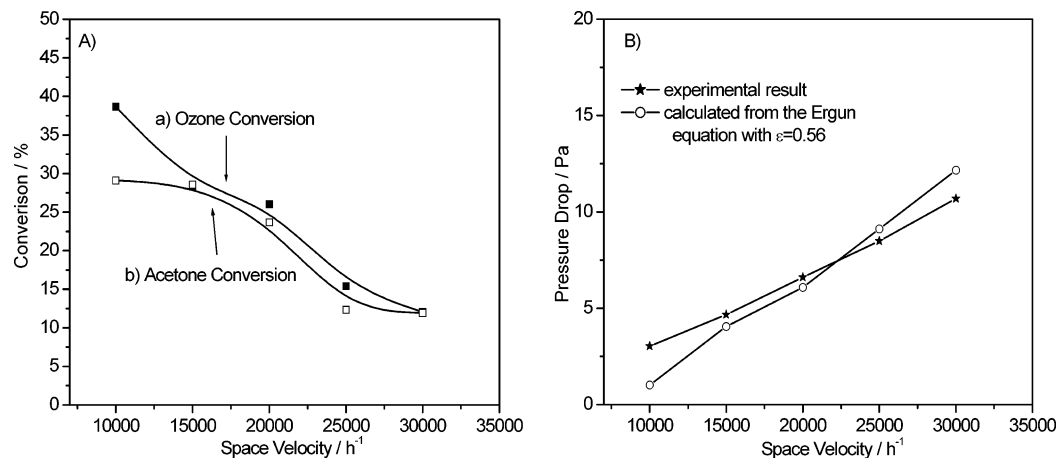


**Figure 9.** (a) Acetone and ozone conversion versus space velocity over 10 wt %  $MnO_x/SiO_2$  at temperature 325 K; (b) pressure drop versus space velocity over 10 wt %  $MnO_x/SiO_2$  at temperature 325 K. Acetone concentration = 1 000 ppm; ozone concentration = 8 000 ppm; space velocity = 10 000–30 000  $h^{-1}$  corresponding to  $F_{tot}$  = 2.1–6.3 L/min.

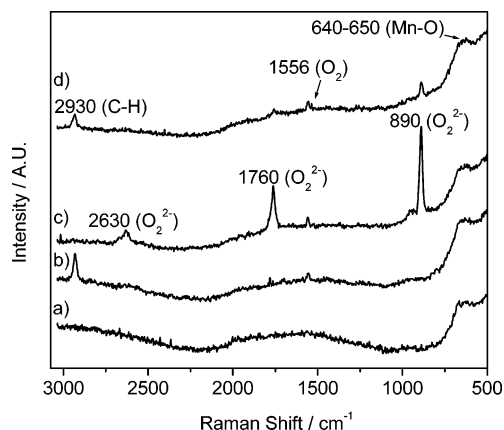


**Figure 10.** Raman spectra of the 10 wt %  $MnO_x/SiO_2$ -H exposed to different gas mixtures at 303 K: (a)  $O_2/He$  (35%  $O_2$ ), (b) acetone/ $O_2/He$  (0.2 mol % acetone, 35 mol %  $O_2$ ), (c)  $O_3/O_2/He$  (1 mol %  $O_3$ , 34 mol %  $O_2$ ), and (d) acetone/ $O_3/O_2/He$  (0.2 mol % acetone, 1 mol %  $O_3$ , 34 mol %  $O_2$ ).

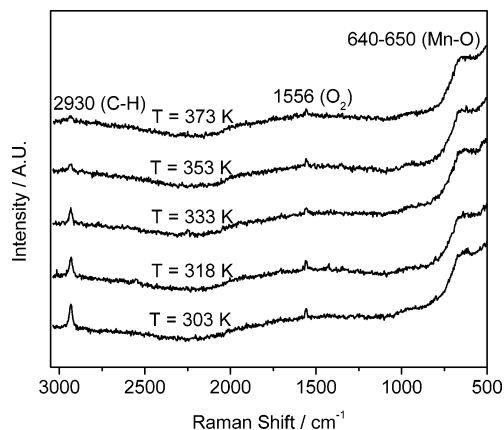


**Figure 11.** Effect of temperature on the 10 wt %  $MnO_x/SiO_2$ -H catalyst in acetone/ $O_2/He$ .

**Raman Spectroscopy Results.** Steady-state, in situ Raman spectroscopy results on the 10 wt %  $MnO_x/SiO_2$ -H catalyst are presented in Figures 10–12. The measurements were successful in characterizing the active phase on the catalyst and identifying two adsorbates on the catalyst surface derived from ozone and acetone. This sample was chosen because it had a high enough surface area to give a significant signal for the adsorbates while maintaining high dispersion.

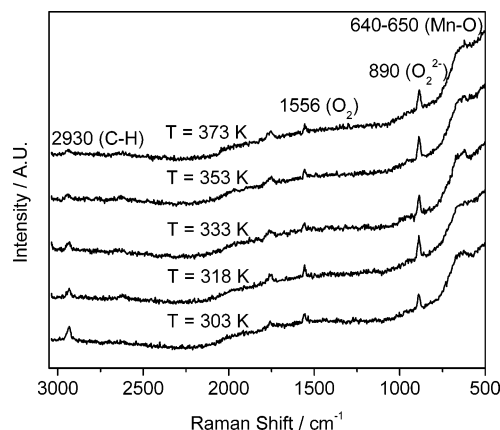


**Figure 12.** Effect of temperature on the 10 wt %  $MnO_x/SiO_2$ -H catalyst in acetone/ $O_3/O_2/He$ .

Figure 10 shows the Raman spectra of the 10 wt %  $MnO_x/SiO_2$ -H catalyst at different reaction conditions. Figure 10a displays the spectrum of a clean catalyst surface with only oxygen and helium flowing over the sample, and shows there is a broad peak in the range of 640–650  $cm^{-1}$ . Figure 10b displays the spectrum of the catalyst when acetone was included in the gas mixture, and shows there is a peak at 2930  $cm^{-1}$ . Figure 10c displays the spectrum of the catalyst surface when only ozone was added to the initial oxygen/helium mixture, and shows a large peak at 890  $cm^{-1}$  and two other peaks at 1760 and 2630  $cm^{-1}$ . Figure 10d displays the spectrum of the catalyst surface under reaction conditions when both acetone and ozone were introduced to the sample simultaneously, and shows that the band associated with the ozone significantly diminished in intensity when acetone and ozone were both in the reaction mixture.

Figure 11 shows the effect of temperature on the acetone adsorption signal at steady-state without the addition of ozone in the feed stream. As shown, the intensity of the adsorbed acetone peak at 2930  $cm^{-1}$  decreased with increasing temperature.

Figure 12 shows the effect of temperature when both acetone and ozone were included in the feed stream. Again, there was a decrease in the intensity of the adsorbed acetone peak with increasing temperature, but the same trend was not seen for the peak at 890  $cm^{-1}$  associated with ozone. The peak associated with ozone actually increased slightly with increasing temperature.



## Discussion

**Structure of the Supported Manganese Oxide.** The XRD analysis of the foam-supported catalysts indicates that the main phase is  $\alpha$ - $\text{Al}_2\text{O}_3$  with a  $\text{ZrO}_2$  component. No discernible peaks due to manganese oxide are visible in the XRD profiles indicating that the active phase is well dispersed. The TPR profiles were similar for the two catalysts with two reduction peaks at 493 and 571 K indicating the presence of similar oxide phases of manganese. They both have the same onset reduction temperature ( $T_{\text{red}} = 443$  K).

Because of the lack of XRD features EXAFS spectroscopy was employed to obtain local structure information for the samples. The Fourier transform profiles of the Mn K-edge EXAFS spectra for those samples gave three distinctive peaks at 0.15, 0.25, and 0.32 nm. The peaks are close to the respective Mn–O and Mn–Mn distances in both  $\text{Mn}_3\text{O}_4$  and  $\beta$ - $\text{MnO}_2$ , but cannot be unequivocally assigned to a particular phase because of the similarity in the distances. The XANES spectra of the samples shows that the  $E_0$  position for the silica-supported sample is close to that of the  $\text{Mn}_3\text{O}_4$ , and the  $E_0$  position for the alumina-supported sample is close to that of the  $\beta$ - $\text{Mn}_2\text{O}_3$ . In another study where silica-supported manganese oxide catalysts of different loadings (3, 10, 15, and 20 wt %) were studied,<sup>26</sup> it was found that with lower loading the oxidation state of the samples was close to  $\beta$ - $\text{Mn}_2\text{O}_3$  while with higher loading the oxidation state was close to  $\text{Mn}_3\text{O}_4$ . It is concluded that the samples here are intermediate between these two states. In that study it was also found that the 10 wt % sample was more active than the 3 wt % sample, so in this work a loading of 10 wt % was chosen for the catalysts. The lower loading sample is less active because the reaction is structure-sensitive, as the complete oxidation of acetone requires many oxygen atoms.

The crystallites, if present, are smaller than 4 nm as no XRD lines are seen. The dispersion of the samples (Table 3) is less than 10%, indicating that the supports are not uniformly covered by a monolayer of manganese oxide. The acidity of the supports may have some influence on the adsorption of the acetone, but the oxidation reaction probably occurs on the  $\text{MnO}_x$  phase, and the acidity probably affects the reactivity indirectly.

**Reactivity Study.** As expected, ozone was a stronger oxidant than oxygen for acetone over both catalysts (Figure 6a,b). As discussed in the Introduction, this is in agreement with the results presented by others.<sup>2,3,5,8,9,18,19</sup> For both the silica- and alumina-supported catalysts the presence of ozone allowed the oxidation of acetone to occur at close to room temperature with the alumina-supported catalyst showing higher activity. On both catalysts the reaction with oxygen began at substantially higher temperatures (475–500 K). Over a blank alumina foam acetone did not react with oxygen but did react with ozone in the gas phase at temperatures higher than 450 K (Figure 6a). The gas-phase reaction of ozone with organic compounds has been well discussed.<sup>27–30</sup> At high temperatures (>425 K) the acetone conversion increased significantly due to the reaction between oxygen and acetone.

Both the  $\text{SiO}_2$ - and  $\text{Al}_2\text{O}_3$ -supported catalysts were active in the decomposition of ozone. Parts a and b of Figure 7 show that ozone decomposed rapidly over the two catalysts at low temperatures (<400 K) and reached complete conversion at 350 K over the  $\text{MnO}_x/\text{SiO}_2$  catalyst and at 400 K over the  $\text{MnO}_x/\text{Al}_2\text{O}_3$  catalyst. The thermal decomposition on the blank foam began only between 400 and 450 K and was complete at close to 550 K.

The behavior of the catalysts in the presence of ozone was peculiar (Figure 6) but can be understood. In both cases the conversions of acetone reached a plateau at about 350 K to further increase above 450 K and join the conversion curves for the reaction with oxygen. The convergence with the oxygen results is expected, since at high temperatures ozone is thermally decomposed and the predominant catalytic pathway is the combustion of acetone with oxygen. The plateau is found exactly at the point (350 K) where ozone conversion is essentially complete. The plateau arises because the acetone reaction at this point is limited by the delivery of oxygen equivalents from ozone and the conversion does not rise. Normally at this point ozone would decompose to molecular oxygen on the catalyst surface. However, the acetone captures active oxygen intermediates and consumes them in its oxidation reaction.

The results in Figure 8 with different ozone/acetone ratios ( $R$ ) can be readily understood from the previous discussion. The figure shows that as the ozone-to-acetone ratio is increased, the conversion of acetone increases while at the same time the breadth of the plateau decreases. Both results are due to the increased availability of oxygen equivalents for the oxidation of acetone. For the alumina-supported catalyst the conversion toward the end of the plateau actually dips before rising again. This occurs on this catalyst because the reaction region extends to higher temperatures than for the silica-supported catalyst where ozone starts decomposing thermally. The conversion rises again at the highest temperatures because the reaction of acetone in that region occurs with oxygen from molecular oxygen.

As expected the pressure drop on the foam catalyst was low and increased with increasing space velocity (Figure 9b). This is in agreement with the results reported by Dhandapani et al.,<sup>12</sup> that a foam or monolith gave a smaller pressure drop than pellets with the same surface area. It was reported that a  $\text{SiC}-\text{Al}_2\text{O}_3$  foam containing 50 wt % alumina with a pore density of 30 ppi had a void fraction of 0.89.<sup>25</sup> But in our results using a void fraction of 0.56 in the theoretical calculation of the Ergun equation gave good agreement with the experimental data (Figure 9b). This void fraction is smaller than the reported one probably due to the coverage of the pores with the washcoats. The small pressure drop indicates that foams are promising supports for applications that require high space velocity. However, the conversion of acetone is not complete, and slightly higher temperatures and higher ozone concentrations are needed.

**Raman Spectra.** Figure 10 shows that all the spectra of the samples have a broad peak in the range of 640–650  $\text{cm}^{-1}$ . This peak is assigned as a manganese oxide mode,<sup>31</sup> but the identification of the exact phase using Raman spectroscopy is difficult due to the similarity in the Raman modes for the various manganese oxide phases in that range. One study summarized the findings of many Raman studies on bulk manganese oxides and reported that  $\beta$ - $\text{MnO}_2$ ,  $\beta$ - $\text{Mn}_2\text{O}_3$ , and  $\text{Mn}_3\text{O}_4$  all have frequencies in the 640–650  $\text{cm}^{-1}$  range.<sup>32</sup> The same study identified the Raman peak located at  $\sim 650$   $\text{cm}^{-1}$  as characteristic of  $\text{Mn}_3\text{O}_4$ , the most Raman active phase of all manganese oxides. The study concluded that the Raman modes found in this range for the  $\beta$ - $\text{MnO}_2$  and  $\beta$ - $\text{Mn}_2\text{O}_3$  samples could actually be attributed to  $\text{Mn}_3\text{O}_4$  formed due to the local heating of the samples during spectrum acquisition. Assuming that there was no local heating due to sample rotation in our experiments, Raman spectroscopy provided support for XRD and EXAFS evidence presented in another study<sup>26</sup> that the most active phase in this catalyst was similar to  $\text{Mn}_3\text{O}_4$ .

The presence of acetone resulted in a peak at 2930  $\text{cm}^{-1}$  (C–H mode) that can be attributed to an adsorbed acetone



species (Figure 10b). The CH<sub>3</sub> symmetric stretching mode for gas-phase acetone appears at  $\sim 2937\text{ cm}^{-1}$ .<sup>33</sup> Also shown in this particular spectrum is a small peak at  $1556\text{ cm}^{-1}$ , which is due to gas-phase oxygen. Since the focal point of the collection lens was at the laser spot on the surface of the catalyst sample, the intensity of peaks due to gas-phase species was expected to be weak. This is confirmed by the small signal for the gas-phase oxygen, which is actually in great excess ( $\sim 1\ 500\%$ ) over ozone. In the presence of ozone there is a large peak at  $890\text{ cm}^{-1}$  (Figure 10c) that was identified in previous isotopic and theoretical work done in our laboratory to be due to a peroxide species (O—O band).<sup>15,16</sup> The features located at  $1760$  and  $2630\text{ cm}^{-1}$  were overtone bands of the  $890\text{ cm}^{-1}$  peak. When both acetone and ozone were introduced to the sample simultaneously, the intensity of the peak for ozone was significantly reduced whereas the intensity of the peak due to acetone was little affected. This indicates that acetone competes with ozone for active catalyst sites, but that its adsorption is equilibrated. Further evidence that shows that acetone adsorption is equilibrated is that the same coverage is obtained regardless of whether the temperature is approached from higher or lower values.

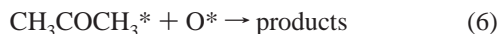
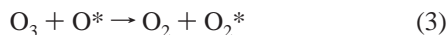
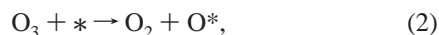
**Mechanism of Reaction.** Comparison of Figure 6b and Figure 7b shows that in the acetone oxidation reaction the TOF of ozone decomposition ( $0.1\text{--}0.2\text{ s}^{-1}$ , maximum) is about  $10\times$  larger than the TOF of acetone oxidation ( $0.01\text{--}0.03\text{ s}^{-1}$ , maximum). The stoichiometry of acetone oxidation, assuming only one active oxygen per ozone molecule is used (maximum ozone consumption), is



Thus, about 20% more ozone is utilized than needed for the oxidation reaction and it is concluded that ozone decomposition occurs in parallel with oxidation.

The relative rates of decomposition of ozone and reaction of ozone with acetone differed on both catalysts. On the 10 wt % MnO<sub>x</sub>/Al<sub>2</sub>O<sub>3</sub> the rate of reaction of ozone with acetone was higher than the rate of decomposition, while on the 10 wt % MnO<sub>x</sub>/SiO<sub>2</sub> the decomposition rate of ozone was slightly higher than the oxidation rate (Figure 7b). This indicates that some of the steps in the reaction sequence occurred at different rates on the catalysts.

The following reaction sequence may be used to understand the behavior of the catalysts. The sequence is presented without proof and there may be other possible steps in the actual mechanism. However, as will be discussed below, several parts of the sequence have been verified separately.



In the sequence the \* denotes surface species, including empty sites.

The first three steps are well established for the decomposition of ozone on manganese oxide catalysts from kinetic, spectroscopic, isotopic, and computational studies.<sup>15,16,34,35</sup> The inclusion of these steps reflects the observation that ozone decom-

position occurs in parallel with the oxidation of acetone. The steps are irreversible, as ozone is not produced on the catalysts and oxygen adsorption does not form peroxide species, O<sub>2</sub><sup>\*</sup>, at any conditions of temperature or pressure. The fourth step is evidenced by in situ Raman studies of acetone oxidation with ozone (Figure 10a), which show the presence of an adsorbed species with intact C—H bonds. The species is likely to be in adsorption equilibrium as its surface concentration is little affected by the presence of ozone. The last step starts a sequence of oxidation steps that leads to full oxidation and reflects the findings that there are no other adsorbed species observed and that CO<sub>2</sub> is the only carbon-containing product of the oxidation. The complete, facile oxidation of the adsorbed acetone once it is attacked by a reactive oxygen species is reasonable, as the molecule becomes activated to further reaction.

A question that remains open is whether the oxidizing species is atomic (O<sup>\*</sup>) or molecular (O<sub>2</sub><sup>\*</sup>). In ozone decomposition the most abundant surface species is the peroxidic, molecular form, which is readily observed by in situ Raman spectroscopy,<sup>15,16,34,35</sup> and this indicates that its decomposition through reaction 4 is a slow step. It is likely though, at least for the alumina-supported catalyst, that the reactive intermediate for acetone oxidation is the atomic form. The reason is the observation that the overall rate of the ozone decomposition reaction is faster in the presence of acetone (Figure 7a). This is unexpected, as the adsorbed acetone competes for sites, and would be expected to retard the reaction. This can be seen from the Raman spectra results in Figure 10d, which showed that acetone significantly reduced the coverage by the peroxide species derived from ozone. However, if the acetone acts as a sink for the oxygen atoms, it could accelerate the usage of ozone by consuming the atoms and freeing up empty sites. The reaction of the oxygen atoms would reduce the concentration of the peroxide intermediates as observed.

## Conclusions

This paper presented a study of acetone oxidation by ozone on manganese oxide catalysts supported on foam substrates. XRD and EXAFS spectroscopies were used to characterize the structure of the catalysts, in situ laser Raman spectroscopy was used to probe surface species, and reactivity measurements were performed to assess the oxidizing power of ozone. The main conclusions are summarized below.

(i) The Fourier transform profiles of the Mn K-edge EXAFS spectra for the supported manganese oxide samples gave three distinctive peaks at 0.15, 0.25, and 0.32 nm and were close to the profiles of Mn<sub>3</sub>O<sub>4</sub> and β-MnO<sub>2</sub>.

(ii) The number of surface active sites was determined through oxygen chemisorption measurements at a reduction temperature ( $T_{\text{red}} = 443\text{ K}$ ) determined from TPR experiments. It was found that the silica-supported catalyst had a larger atomic oxygen uptake than the alumina-supported catalyst.

(iii) In situ steady-state Raman spectroscopy measurements during acetone catalytic oxidation showed the presence of an adsorbed acetone species with a C—H bond at  $2930\text{ cm}^{-1}$  and a peroxide species derived from ozone with a bond at  $890\text{ cm}^{-1}$ .

(iv) The adsorption of the acetone species was equilibrated, but the adsorption of the peroxide intermediate was not and was reduced by the presence of acetone.

(v) The introduction of ozone reduced the reaction temperature for acetone catalytic oxidation on both the alumina- and silica-supported catalysts. The alumina-supported catalyst was found to be more active with higher turnover frequencies (TOFs)

compared to the silica-supported catalyst in the acetone oxidation and ozone decomposition reactions.

(vi) For the foam-supported catalyst the pressure drop was small and indicated that the foams are promising materials as catalyst supports in high flow rate applications such as air pollution control.

**Acknowledgment.** We gratefully acknowledge the financial support for this work by the Director of the Division of Chemical and Thermal Systems of the National Science Foundation (Grant CTS-9815041) and Brookhaven National Laboratory (Grant 3972).

## Appendix

The acetone vapor pressure was calculated by Antoine's equation

$$y_v = \frac{P_v}{P_{\text{tot}}} = \frac{10^{(A - [B/(T+C)])}}{P_{\text{tot}}} \quad (7)$$

where  $P_v$  and  $P_{\text{tot}}$  are the vapor pressure and total pressure in units of Torr;  $T$  is temperature in units of °C;  $y_v$  is the partial vapor pressure fraction; and  $A$ ,  $B$ , and  $C$  are the Antoine coefficients for acetone with values equal to 7.02447, 1161, and 224, respectively.

The pressure drop calculations were carried out using the Ergun equation modified for foams<sup>25</sup>

$$\Delta P = \frac{\mu L}{k_1} v_s + \frac{\rho L}{k_2} v_s^2 \quad (8)$$

$$k_1 = \frac{\epsilon^3 d_p^2}{150(1 - \epsilon)^2} \quad (9)$$

$$k_2 = \frac{\epsilon^3 d_p}{1.75(1 - \epsilon)} \quad (10)$$

where  $\mu$  is the viscosity of the fluid (for air at 325 K,  $\mu = 1.95 \times 10^{-5}$  N s/m<sup>2</sup>),  $\rho$  is the density of the fluid (for air at 325 K,  $\rho = 1.09$  kg/m<sup>3</sup>),  $v_s$  is the average fluid velocity (internal velocity through the foam),  $L$  is the height of the fixed bed (for the ceramic foam,  $L = 1.3$  cm),  $d_p$  is the diameter of the particles in the bed, and  $\epsilon$  is the void fraction. For ceramic foams  $d_p$  can be defined as

$$d_p = 1.5 \frac{(1 - \epsilon)}{\epsilon} d_c \quad (11)$$

where  $d_c$  is the diameter of the pore in the foam. The foam of 30 ppi pore density has a corresponding  $d_c$  of 0.085 cm, and the void fraction of the silica-coated foam is approximately 0.56

calculated from the Ergun equation through nonlinear regression fitting, using Polymath 5.0 software.

## References and Notes

- (1) Hunter, P.; Oyama, S. T. *Control of Volatile Organic Compound Emissions, Conventional and Emerging Technologies*; John Wiley & Sons: New York, 2001.
- (2) Gervasini, A.; Vezzoli, G. C.; Ragaini, V. *Catal. Today* **1996**, *29*, 449.
- (3) Gervasini, A.; Binachi, C. L.; Ragaini, V. In *Environmental Catalysis*; Armor, J. N., Ed.; ACS Symp. Ser. 552; American Chemical Society: Washington, DC, 1994; p 352.
- (4) Li, W.; Oyama, S. T. In *Heterogeneous Hydrocarbon Oxidation*; Warren, B. K., Oyama, S. T., Eds.; ACS Symp. Ser. 638; American Chemical Society: Washington, DC, 1996; p 364.
- (5) Ragaini, V.; Bianchi, C. L.; Forcella, G.; Gervasini, A. In *Trends in Ecological Physical Chemistry*; Bonati, L., Ed.; Elsevier: Amsterdam, The Netherlands, 1993; p 275.
- (6) Kastrer, J. R.; Buqusi, Q.; Ganagavaram, R.; Das, K. C. *Environ. Sci. Technol.* **2005**, *39*, 1835.
- (7) Wojtowicz, J. A. Ozone. In *Kirk-Othmer Encyclopedia of Chemical Technology*, 4th ed.; John Wiley & Sons: New York, 1996; p 953.
- (8) Naydenov, A.; Mehandjiev, D. *Appl. Catal. A* **1993**, *97*, 17.
- (9) Oyama, S. T.; Li, W.; Zhang, W. *Stud. Surf. Sci. Catal.* **1999**, *121*, 105.
- (10) Hutchings, G. J.; Scurrall, M. S.; Woodhouse, J. R. *Appl. Catal.* **1988**, *38*, 157.
- (11) Paulis, M.; Gandía, L. M.; Gil, A.; Sambeth, J.; Odriozola, J. A.; Montes, M. *Appl. Catal. B* **2000**, *26*, 37.
- (12) Dhandapani, B.; Oyama, S. T. *Appl. Catal. B* **1997**, *11*, 129.
- (13) Borekov, G. K. In *J. R. Anderson; Catalysis Science and Technology*; Boudart, M. B., Ed.; Springer: Berlin, Germany, 1982; Vol. 3, p 39.
- (14) Kim, S. C. *J. Hazard. Mater. B* **2002**, *91*, 285.
- (15) Li, W.; Gibbs, G. V.; Oyama, S. T. *J. Am. Chem. Soc.* **1998**, *120*, 9041.
- (16) Li, W.; Oyama, S. T. *J. Am. Chem. Soc.* **1998**, *120*, 9047.
- (17) Gil, A.; Burgos, N.; Paulis, M.; Montes, M.; Gandía, L. M. *Stud. Surf. Sci. Catal.* **2000**, *130*, 2153.
- (18) Parida, K. M.; Samal, A. *Appl. Catal. A* **1999**, *182*, 249.
- (19) Baldi, M.; Finocchio, E.; Milella, F.; Busca, G. *Appl. Catal. B* **1998**, *16*, 43.
- (20) Lu, T. J.; Stone, H. A.; Ashby, M. F. *Acta Metall. Mater.* **1998**, *46*, 3619.
- (21) Dietz, A. G., III; Carlsson, A. F.; Schmidt, L. D. *J. Catal.* **1996**, *176*, 459.
- (22) Huff, M.; Schmidt, L. D. *J. Catal.* **1995**, *155*, 82.
- (23) DeLuca, J. P.; Campbell, L. E. In *Monolithic Catalyst Supports, Advanced Materials in Catalysis*; Burton, J. J., Garten, R. L., Eds.; Academic Press: New York, 1977.
- (24) Patcas, F. C. *J. Catal.* **2005**, *231*, 194.
- (25) Innocentini, M. D. M.; Salvini, V. R.; Macedo, A.; Pandolfelli, V. C. *Mater. Res.* **1999**, *2* (4), 283.
- (26) Reed, C.; Xi, Y.; Lee, Y.-K.; Oyama, S. T. *J. Phys. Chem. B* Submitted for publication.
- (27) Bailey, P. S. *Ozonation in Chemistry*; Academic Press: New York, 1978; Vol. 1.
- (28) Bailey, P. S. *Ozonation in Chemistry*; Academic Press: New York, 1978; Vol. 2.
- (29) Atkinson, R.; Carter, W. P. L. *Chem. Rev.* **1987**, *84*, 437.
- (30) Oyama, S. T. *Catal. Rev. Sci. Eng.* **2000**, *42*, 279.
- (31) Kapteijn, F.; van Langeveld, A. D.; Moulijn, J. A.; Andreini, A.; Vuurman, M. A.; Turek, A. M.; Jehng, J. M.; Wachs, I. E. *J. Catal.* **1994**, *150*, 94.
- (32) Buciuman, F.; Patcas, F.; Craciun, R.; Zahn, D. R. T. *Phys. Chem. Chem. Phys.* **1999**, *1*, 185.
- (33) Chu, P. M.; Guenther, F. R.; Rhoderick, G. C.; Lafferty, W. J. Quantitative Infrared Database, in NIST Chemistry WebBook, <http://webbook.nist.gov/cgi/cbook.cgi>; No. 69, June 2005 release.
- (34) Radhakrishnan, R.; Oyama, S. T.; Chen, J. G.; Asakura, K. *J. Phys. Chem. B* **2001**, *105*, 4245.
- (35) Radhakrishnan, R.; Oyama, S. T. *J. Catal.* **2001**, *199*, 282.